

Analysis of multiple reflection effects in reflective measurements of electro-optic coefficients of poled polymers in multilayer structures

Dong Hun Park, Chi H. Lee, and Warren N. Herman

Laboratory for Physical Sciences, Department of Electrical Engineering, University of Maryland, College Park
20740, USA

leomac@umd.edu, chlee@umd.edu, herman@lps.umd.edu

Abstract: We present new closed-form expressions for analysis of Teng-Man measurements of the electro-optic coefficients of poled polymer thin films. These expressions account for multiple reflection effects using a rigorous analysis of the multilayered structure for varying angles of incidence. The analysis based on plane waves is applicable to both transparent and absorptive films and takes into account the properties of the transparent conducting electrode layer. Methods for fitting data are presented and the error introduced by ignoring the transparent conducting layer and multiple reflections is discussed.

©2006 Optical Society of America

OCIS codes: (190.4710) Optical nonlinearities in organic materials; Electro-optic polymers; (310.6860) Thin films, optical properties.

References and links

1. G. A. Lindsay and K. D. Singer, eds., *Polymers for Second-Order Nonlinear Optics*, (ACS Symposium Series 601, 1995).
2. D. M. Burland, R. D. Miller, and C. A. Walsh, "Second-order nonlinearity in poled-polymer systems," *Chem. Rev.* **94**, 31–75 (1994).
3. M. A. Mortazavi, A. Knoesen, S. T. Kowel, B. G. Higgins, and A. Dienes, "Second-harmonic generation and absorption studies of polymer-dye films oriented by corona-onset poling at elevated temperatures," *J. Opt. Soc. Am. B* **6**, 733-741 (1989).
4. R. A. Norwood, M. G. Kuzyk, and R. A. Keosian, "Electro-optic tensor ratio determination of side-chain copolymers with electro-optic interferometry," *J. Appl. Phys.* **75**, 1869-1874 (1994).
5. Y.-P. Wang, J.-P. Chen, X.-W. Li, J.-X. Hong, X.-H. Zhang, J.-H. Zhou, and A.-L. Ye, "Measuring electro-optic coefficients of poled polymers using fiber-optic Mach-Zehnder interferometer," *Appl. Phys. Lett.* **85**, 5102-5103 (2004).
6. M. J. Shin, H. R. Cho, S. H. Han, and J. W. Wu, "Analysis of Mach-Zehnder interferometry measurement of the Pockels coefficients in a poled polymer film with a reflection configuration," *J. Appl. Phys.* **83**, 1848-1853 (1998).
7. H. Uchiki and T. Kobayashi, "New determination method of electro-optic constants and relevant nonlinear susceptibilities and its application to doped polymer," *J. Appl. Phys.* **64**, 2625-2629 (1988).
8. D. Morichère, P.-A. Chollet, W. Fleming, M. Jurich, B. A. Smith, and J. D. Swalen, "Electro-optic effects in two tolane side-chain nonlinear-optical polymers: comparison between measured coefficients and second-harmonic generation," *J. Opt. Soc. Am. B* **10**, 1894-1900 (1993).
9. L. M. Hayden, G. F. Sauter, F. R. Ore, P. L. Pasillas, J. M. Hoover, G. A. Lindsay, and R. A. Henry, "Second-order nonlinear optical measurements in guest-host and side-chain polymers," *J. Appl. Phys.* **68**, 456-465 (1990).
10. S. Kalluri, S. Garner, M. Ziari, W. H. Steier, Y. Shi, and L. R. Dalton, "Simple two-slit interference electro-optic coefficients measurement technique and efficient coplanar electrode poling of polymer thin films," *Appl. Phys. Lett.* **69**, 275-277 (1996).
11. C. C. Teng and H. T. Man, "Simple reflection technique for measuring the electro-optic coefficient of poled polymers," *Appl. Phys. Lett.* **56**, 1734-1736 (1990).
12. J. S. Schildkraut, "Determination of the electro optic coefficient of a poled polymer film," *Appl. Opt.* **29**, 2839-2841 (1990).

13. K. Clays and J. S. Schildkraut, "Dispersion of the complex electro-optic coefficient and electrochromic effects in poled polymer films," *J. Opt. Soc. Am. B* **9**, 2274-2282 (1992).
14. P. M. Lundquist, M. Jurich, J.-F. Wang, H. Zhou, T. J. Marks, and G. K. Wong, "Electro-optic characterization of poled-polymer films in transmission," *App. Phys. Lett.* **69**, 901-903 (1996).
15. F. Michelotti, A. Belardini, M. C. Larciprete, M. Bertolotti, A. Rousseau, A. Ratsimihety, G. Schoer, and J. Mueller, "Measurement of the electro-optic properties of poled polymers at $\lambda = 1.55 \mu\text{m}$ by means of sandwich structures with zinc oxide transparent electrode," *Appl. Phys. Lett.* **83**, 4477-4479 (2003).
16. Y. Levy, M. Dumont, E. Chastaing, P. Robin, P.-A. Chollet, G. Gadret, and F. Kajzar, "Reflection method for electro-optical coefficient determination in stratified thin film structures," *Mol. Cryst. Liq. Cryst. Sci. Technol. Sect. B* **4**, 1-19 (1993).
17. P.-A. Chollet, G. Gadret, F. Kajzar and P. Raimond, "Electro-optic coefficient determination in stratified organized molecular thin films: application to poled polymers," *Thin Solid Films*, **242**, 132-138 (1994).
18. G. Khanarian, J. Sounik, D. Allen, S. F. Shu, C. Walton, H. Goldberg and J. B. Stamatoff, "Electro-optic characterization of nonlinear-optical guest-host films and polymers," *J. Opt. Soc. Am. B* **13**, 1927-1934 (1996)
19. S. H. Han and J. W. Wu, "Single-beam polarization interferometry measurement of the linear electro-optic effect in poled polymer films with a reflection configuration," *J. Opt. Soc. Am. B* **14**, 1131-1137 (1997).
20. F. Michelotti, G. Nicolao, F. Tesi, and M. Bertolotti, "On the measurement of the electro-optic properties of poled side-chain copolymer films with a modified Teng-Man technique," *Chem. Phys.* **245**, 311-325 (1999).
21. Y. Shuto and M. Amano, "Reflection measurement technique of electro-optic coefficients in lithium niobate crystals and poled polymer films," *J. Appl. Phys.* **77**, 4632-4638 (1995).
22. I. P. Kaminow, *An Introduction to Electrooptic Devices*, (Academic Press, Inc., 1974).
23. F. Wang, E. Furman, and G.H. Haertling, "Electro-optic measurements of thin-film materials by means of reflection differential ellipsometry," *J. App. Phys.* **78**, 9-15 (1995).
24. D. Guo, R. Lin, and W. Wang, "Gaussian-optics-based optical modeling and characterization of a Fabry-Perot microcavity for sensing applications," *J. Opt. Soc. Am. A* **22**, 1577-1588 (2005).
25. M. Born and E. Wolf, *Principles of Optics*, 7th ed. (Cambridge University Press, 1999).
26. For a discussion of wave impedances, see, for example, Ramo, Whinnery, and Van Duzer, *Fields and Waves in Communication Electronics*, (John Wiley and Sons, New York, 1965), Chap. 6.
27. M. T. Heath, *Scientific Computing*, 2nd ed. (McGraw Hill, 2002).
28. R. A. Synowicki, "Spectroscopic ellipsometry characterization of indium tin oxide film microstructure and optical constants," *Thin Solid Films*, 313-314, 394-397 (1998).

1. Introduction

Organic molecules have attracted great interest for their potential applications in nonlinear optical (NLO) devices. In particular, poled polymers based on second-order nonlinearity have been widely studied because they are a class of photonic material that may substitute for inorganic nonlinear crystals in high speed optical communication and signal processing [1].

Obtaining a macroscopic 2nd order NLO response requires orientation of the chromophores, which can be achieved by electric field poling [2]. Corona [3] and electrode contact poling techniques are usually used. Methods of measuring the linear electro-optic (EO) effect include Mach-Zehnder (MZ) interferometry [4-6], Fabry-Perot (FP) interferometry [7], attenuated total reflection [8] (ATR), waveguide method [9], and two slit interference method [10]. One of the most popular measurement techniques is a reflection method introduced by Teng and Man [11] (Teng-Man) as well as by Schildkraut [12]. The reflection measurement is generally easier to make compared to techniques such as MZ interferometry because it simply takes advantage of a relative phase-shift difference between the *s*- and *p*- polarized waves of a single laser beam reflected from the sample when a modulating voltage is applied across two parallel-plate electrodes. A transmission method was first mentioned by Schildkraut [12,13], and later discussed in some detail by Lundquist, *et al.* [14] This method, which also measures a relative phase-shift, affords a somewhat simpler alignment compared to the reflection method, but requires two transparent electrodes.

Many researchers have been synthesizing chromophores for incorporation into polymeric materials to achieve high nonlinearity in a poled polymer thin film. The EO properties are often characterized using the Teng-Man reflection method because it is simple and quick. The vast majority of quoted values of the electro-optic coefficient that are obtained from Teng-

Many measurements result from a simplified analysis of the data that assumes the transparent conducting oxide (TCO) is perfectly transparent and the gold is perfectly reflective. Consequently only the properties of the EO material [refractive indices (sometimes anisotropic), EO coefficients, and angle of incidence] are taken into account. However, in both Refs. 11 and 12, it was realized that experimental error can result from ignoring the reflection off the substrate-film interface and that an accurate determination of the EO coefficient could be achieved only by numerical calculation that applies anisotropic Fresnel equations to the stratified layers containing the nonlinear poled polymer. This requires knowledge of the refractive index and thickness of all the layers. In addition, the simple analysis is valid only when the absorption of the film is negligible. Furthermore, Michelotti, *et al.* [15] reported that the simple Teng-Man analysis can give unreliable measurements if the experimental setup is operated in a spectral region where the TCO layer is absorbing, and suggested that if it is only slightly absorbing it is still possible to evaluate the EO properties of the polymer films with reasonable precision.

The effect of electrochromism (variation of the imaginary part of the index of refraction under application of an electric field) and the complex EO coefficient was added in Ref. 13, followed by efforts by a few researchers to characterize other nonlinear properties, such as the complex quadratic EO coefficient, based on a simple analysis of Teng-Man data [20].

Levy, *et al.* [16] and Chollet, *et al.* [17] presented both simple and rigorous expressions for estimation of the complex EO coefficient. Numerical solutions to the rigorous expressions were obtained using the simplex method. They also pointed out that the modulated intensity at the maximum of the optical bias curve and some of the modulation dependence on angle of incidence are attributed to absorption of the film and to multiple reflections, respectively. Ignoring multiple reflections inside the polymer film, Khanarian, *et al.* [18] derived an approximate equation for the real part of the EO coefficient that takes into account the effects of reflectivity modulation at the glass/polymer and polymer/metal interfaces. Han and Wu [19] measured the modulated intensity as a function of optical bias, optical polarization, and angle of incidence in an effort to distinguish FP effects from EO phase modulation.

In this paper, we provide new closed-form expressions for analysis of Teng-Man data including absorption of both the film and TCO layers. The analysis also applies to any uniaxial nonlinear thin film with the *c*-axis perpendicular to the nonlinear film surface, such as thin *z*-cut Lithium Niobate. In general the modulation of both the real and imaginary parts of the complex refractive index under application of an electric field depends on both the real and imaginary parts of the complex EO coefficient, particularly inside the linear absorption band of the polymer [13]. Two models, both allowing for absorption of the nonlinear polymer layer, are analyzed and compared: a simple model that takes into account only the properties of the nonlinear polymer layer without multiple reflections and a rigorous model accounting for properties of the complete stratified layers of the test structure including multiple reflections. In both models, analytic expressions that are linearly dependent on the real and imaginary parts of the complex EO coefficient are presented so that standard linear least squares data analysis can be performed. In the case of the simple model, we obtain equations to characterize the imaginary part of the complex EO coefficients that are somewhat different from those reported earlier [13, 16, 20] as well as an identical equation to that usually used in the Teng-Man method for the real part [21] outside the absorption band of the polymer. The rigorous model has the same fundamental starting point as that of Ref. [16], namely, the description of the total reflectivity of the multilayer structure. But we provide explicit analytic expressions for all derivatives involved along with a new compact formalism that allows a matrix representation of the dependence of the real and imaginary parts of the complex EO coefficient on the reflectivity and phase modulation. The rigorous model analysis is used to show that simple model calculations, which do not include the effects of multiple reflections, can, in some cases, either grossly underestimate or overestimate the complex electro-optic coefficient. In addition, it is shown that the relative error in using the simple model can undergo a large cyclic variation, an asymptotic behavior, or an irregular FP effect with increasing film thickness depending on operating wavelength.

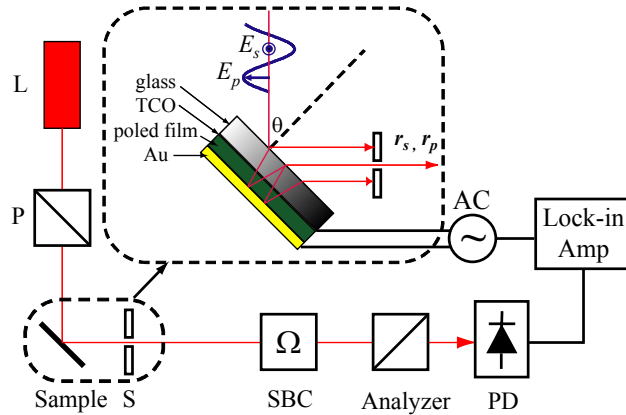


Fig. 1. Schematic of the experimental Teng-Man setup. L is laser, P polarizer, A aperture, S slit, SBC Soleil-Babinet Compensator, and PD photodetector.

2. Theory

A poled organic thin film prepared by spin coating belongs to the point-group symmetry ∞mm (space group $C_{\infty v}$) [22] and has complex ordinary and extraordinary indices of refraction, $\tilde{n}_o = n_o + i\kappa_o$ and $\tilde{n}_e = n_e + i\kappa_e$, respectively. Two independent complex electro-optic tensor elements $\tilde{r}_{13} = r_{13} + is_{13}$ and $\tilde{r}_{33} = r_{33} + is_{33}$ determine the variations $\delta\tilde{n}_o$ and $\delta\tilde{n}_e$ of the complex refractive indices when an electric field E_3 is applied to the film according to [13]

$$\delta\tilde{n}_\mu = -\frac{1}{2}\tilde{n}_\mu^3(r_{\mu 3} + is_{\mu 3})E_3, \quad (1)$$

where $\mu = 1$ or 3 ($n_1 = n_o$ and $n_3 = n_e$). For a parallel plate structure, $E_3 = V/d$, where V is the peak voltage of the AC signal applied to the sample and d is the thickness of the film. Usually it is argued that the real part, δn_μ , of $\delta\tilde{n}_\mu$ depends only on $r_{\mu 3}$ and the imaginary part, $\delta\kappa_\mu$, depends only on $s_{\mu 3}$ outside the polymer absorption band under the assumptions that $n \gg \kappa$, $n\delta\kappa \gg \kappa\delta n$ [13] and $\kappa\delta\kappa \ll n\delta n$. A detailed description of the separation of Eq. (1) into real and imaginary parts is given in Appendix A, where we show that this simplification is not valid when the measurement wavelength is in the absorption band of the film.

2.1 General Expressions

As shown in Fig. 1, light polarized at 45° is incident at an angle on the multilayered sample structure containing the nonlinear poled thin film. The polymer material is usually spin-coated on a glass substrate coated with a TCO, commonly indium tin oxide (ITO), and poled electrically to generate the second order nonlinearity. The first reflection off the air-glass interface and subsequent beams resulting from reflection of the first pass on its way out at the glass-air interface back into the polymer and out again are blocked [11-13]. The remaining light reflected off the sample experiences an additional controllable phase retardation Ω introduced by a Soleil-Babinet Compensator (SBC). The intensity of the light is detected after passing through the analyzer using a lock-in amplifier. At each angle of incidence, two different data sets, the optical bias curve $I_{dc}(\Omega)$ and the modulated intensity $I_m(V, \Omega)$ are collected. The optical bias curve is the intensity profile obtained by varying the retardation generated by the SBC with no application of voltage to the sample, while the modulation data

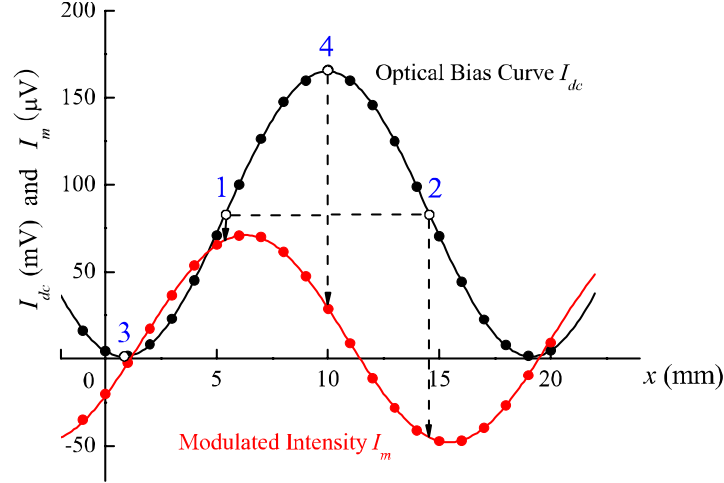


Fig. 2. The optical bias curve and modulated intensity obtained as a function of SBC retardation setting x for a representative set of experimental data on a film with $r_{33} = 42$ pm/V and $s_{33} = 0.3$ pm/V using a peak voltage of 4 V. Points 1, 2, 3, and 4 correspond to compensator settings such that $\Psi_{sp} + \Omega = \pi/2, 3\pi/2, 0,$ and π .

set is obtained by applying an AC voltage $V \sin(\omega t)$ to the sample and using a lock-in amplifier synced to the fundamental frequency of the applied voltage to record the resulting modulation of $I_{dc}(\Omega)$ for a given retardation. $I_{dc}(\Omega)$ can be expressed in terms of the complex reflection coefficients r_s and r_p of the s - and p - polarized waves, the intensity of the incident laser I_o , and the retardation in the form [15-17]

$$I_{dc} = \frac{I_o}{4} |r_s e^{i\Omega} - r_p|^2 = A + B \sin^2 \left(\frac{\Psi_{sp} + \Omega}{2} \right), \quad (2)$$

where

$$A = \frac{I_o}{4} (|r_s| - |r_p|)^2, \quad B = I_o |r_s| |r_p|, \quad (3)$$

$$r_s = |r_s| e^{i\Psi_s}, \quad r_p = |r_p| e^{i\Psi_p}, \quad (4)$$

and

$$\Psi_{sp} = \Psi_s - \Psi_p. \quad (5)$$

To first order in V , the modulated intensity $I_m(V, \Omega)$ is obtained by differentiating Eq. (2) to get

$$I_m = \delta A + \delta B \sin^2 \left(\frac{\Psi_{sp} + \Omega}{2} \right) + \frac{B}{2} \sin(\Psi_{sp} + \Omega) \delta \Psi_{sp}. \quad (6)$$

Representative data curves for optical bias I_{dc} and modulation I_m are shown in Fig. 2. We note in general that I_m is not symmetric with respect to the horizontal axis and the modulated intensities at points 1 and 2 are not maximum and minimum, respectively. From Eq. (6), $\delta \Psi_{sp}$ can be extracted by measuring the modulated intensities I_{m1} and I_{m2} at the two optical bias points corresponding to $\Psi_{sp} + \Omega = \pi/2, 3\pi/2$ as

$$\delta\Psi_{sp} = \frac{I_m(\pi/2) - I_m(3\pi/2)}{2I_c}, \quad (7)$$

where $I_c = B/2$. $\delta B/B$ can be obtained from the modulated intensities I_{m3} and I_{m4} at the two bias points corresponding to $\Psi_{sp} + \Omega = 0, \pi$ according to

$$\frac{\delta B}{B} = \frac{I_m(\pi) - I_m(0)}{2I_c}. \quad (8)$$

Typically, in the Teng-Man method, I_m is measured only at points 1 and 2 as a function of voltage and the average of the difference in the slopes in plots of I_m versus V is used in Eq. (7) to extract $\delta\Psi_{sp}$. This verifies that the applied voltage is low enough to stay in the linear regime, as required for the validity of Eq. (7). Usually, I_m is positive at point 1 and negative at point 2. But this is not always the case so care must be taken to note the phase of the reading on the lock-in amplifier, synced to the fundamental frequency of the applied voltage $V \sin(\omega t)$ (in our case, 1 kHz). A similar technique can be applied to obtain $\delta B/B$ from data at points 3 and 4 using Eq. (8).

To measure modulated intensities at only points 1 and 2 in Fig. 2, an often employed quick measurement technique is to a) vary the compensator to determine the minimum I_{dc} (point 3) and maximum I_{dc} (point 4), b) set the compensator to obtain the average of these two intensities to locate point 1 and measure I_{m1} , c) dial the compensator through the maximum to the same dc average on the other side to locate point 2 and measure I_{m2} , and finally d) use Eq. (7) to determine $\delta\Psi_{sp}$. This can be expected to give as accurate a value for $\delta\Psi_{sp}$ as fitting a full modulation curve, provided multiple measurements are averaged. However, to measure $\delta B/B$ using Eq. (8) requires precisely locating the maximum and minimum in the bias curve, but these are points where the slope of I_{dc} versus Ω is zero. One can show that for a small error $\Delta\Omega$ in the compensator setting in locating points 3 and 4, the relative error in $\delta B/B$ from using Eq. (8) is $-\left[\delta\Psi_{sp}/(\delta B/B)\right]\Delta\Omega$. With moderate reflectivity modulation and $(\delta B/B)/\delta\Psi_{sp} \approx 1$ (higher ratios are possible), and if the error in determining the maximum I_{dc} is only 1% corresponding to $\Delta\Omega \approx 0.2$, then the relative error in determination of $\delta B/B$ is already 20%. Better accuracy can be obtained by fitting the full I_{dc} versus Ω curve to reduce $\Delta\Omega$.

After verifying voltage values to be in the linear regime, we prefer to measure the full $I_m(V, \Omega)$ curves [15,20] as well as $I_{dc}(\Omega)$ as shown in Fig. 2 and then fit these data to Eqs. (2) and (6) to extract $A, B, \Psi_{sp}, \delta A, \delta B$, and $\delta\Psi_{sp}$. Acquiring the full modulation curve provides a visual check for consistency as well as improved statistics on the extracted parameters. Note that in fitting the optical bias curve we put $\Psi_{sp} + \Omega \rightarrow cx + d$, where x is the SBC setting, and obtain c and d along with A and B from the fit. These are then used in fitting Eq. (6) to extract $\delta A, \delta B$, and $\delta\Psi_{sp}$.

To facilitate relating these parameters to the complex EO coefficients, we define a new complex parameter \tilde{B} as

$$\tilde{B} \equiv I_o r_s r_p^* = B e^{i\Psi_{sp}} \quad (9)$$

so that

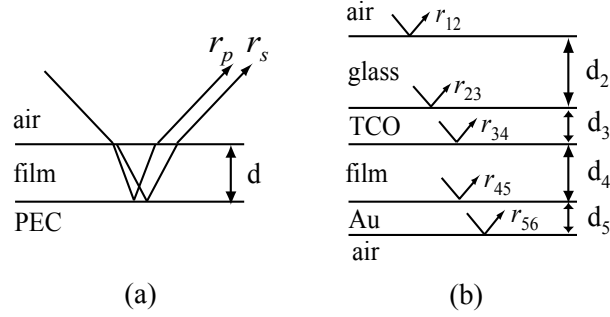


Fig. 3. Multilayered structures in a simple model (a) and a rigorous model (b). For simplicity, subscripts s and p in the reflection coefficients are omitted in (b).

$$\frac{\delta \tilde{B}}{\tilde{B}} = \frac{\delta B}{B} + i \delta \Psi_{sp} = \frac{\delta r_s}{r_s} + \left(\frac{\delta r_p}{r_p} \right)^* \quad (10)$$

Thus, the modulated reflectivity and phase are just the real and imaginary parts, respectively, of $\delta \tilde{B} / \tilde{B}$.

From Eq. (10), assuming $\tilde{r}_{13} = \gamma \tilde{r}_{33}$ (γ is generally assumed to be 1/3 for weak poling [2]), assuming no piezoelectric contribution and making a Taylor expansion to first order in $\delta \tilde{n}_{o,e}$, the complex quantity $\delta \tilde{B} / \tilde{B}$ can be written as a linear function of r_{33} and s_{33} in the form

$$\frac{\delta \tilde{B}}{\tilde{B}} = \frac{1}{r_s} \frac{\partial r_s}{\partial \tilde{n}_o} \delta \tilde{n}_o + \left(\frac{1}{r_p} \frac{\partial r_p}{\partial \tilde{n}_o} \delta \tilde{n}_o + \frac{1}{r_p} \frac{\partial r_p}{\partial \tilde{n}_e} \delta \tilde{n}_e \right)^* \equiv H_r r_{33} + i H_s s_{33} \quad (11)$$

Separating into real and imaginary parts, we have

$$\begin{pmatrix} \delta \Psi_{sp} \\ \frac{\delta B}{B} \end{pmatrix} = \begin{pmatrix} \text{Im}(H_r) & \text{Re}(H_s) \\ \text{Re}(H_r) & -\text{Im}(H_s) \end{pmatrix} \begin{pmatrix} r_{33} \\ s_{33} \end{pmatrix} \quad (12)$$

We note in general that the ratio r_{13}/r_{33} is not equal to $\delta n_o/\delta n_e$ because of birefringence and that both $\delta \Psi_{sp}$ and $\delta B/B$ depend on both r_{33} and s_{33} . Once $\delta \Psi_{sp}$ and $\delta B/B$ are determined experimentally at any single angle of incidence, Eq. (12) can be inverted to solve for r_{33} and s_{33} provided H_r and H_s that determine the 2×2 matrix are known. This matrix depends on the linear properties of the multilayered structure and its form for the simple and rigorous models is discussed in the next two sections.

2.2 Simple Model

The simple model ignores the properties of the TCO layer and simplifies the multilayered structure of the sample to three layers, air-film-PEC (Perfect Electric Conductor), as shown in Fig. 3(a). By also ignoring the reflectance at the air-film interface, the reflection coefficients of the s - and p - waves can be expressed as

$$r_s = -e^{2i\beta_s d}, \quad r_p = -e^{2i\beta_p d} \quad (13)$$

where the propagation constants of the s - and p - waves normal to the film surface are defined as

$$\beta_s = k_o \tilde{n}_s \cos(\tilde{\theta}_s), \quad \beta_p = k_o \tilde{n}_p \cos(\tilde{\theta}_p). \quad (14)$$

Here, $k_o = 2\pi/\lambda$ is the wave vector in free space, $\tilde{n}_s = \tilde{n}_o$, \tilde{n}_p is given in Eq. (B2), and $\tilde{\theta}_s$ and $\tilde{\theta}_p$ are the complex propagation angles inside the anisotropic nonlinear medium. Inserting Eq. (13) into the general expression Eq. (2) gives the optical bias curve. We introduce lower-case letters a , b , and ψ_{sp} instead of A , B , and Ψ_{sp} to designate the simple model values. We emphasize the complex nature of the propagation constants $\beta_{s,p}$ by writing $\beta_s \equiv \beta_{sr} + i\beta_{si}$ and $\beta_p \equiv \beta_{pr} + i\beta_{pi}$. Then, the phase retardation inside the film is given by

$$\psi_{sp} = 2(\beta_{sr} - \beta_{pr})d, \quad (15)$$

which is purely real. In this simple model, the coefficients a and b depend only on the imaginary parts of the propagation constants, while ψ_{sp} depends only on the real parts.

From Eqs. (2)-(6) together with Eq. (15), we have

$$\delta\psi_{sp} = 2(\delta\beta_{sr} - \delta\beta_{pr})d \quad (16)$$

and

$$\delta b = -2b(\delta\beta_{si} + \delta\beta_{pi})d. \quad (17)$$

Inserting Eq. (13) into the general expression Eq. (11), we have

$$\frac{\delta\tilde{b}}{\tilde{b}} = \frac{\delta b}{b} + i\delta\psi_{sp} = 2id \left[\frac{\partial\beta_s}{\partial\tilde{n}_o} \delta\tilde{n}_o - \left(\frac{\partial\beta_p}{\partial\tilde{n}_o} \delta\tilde{n}_o + \frac{\partial\beta_p}{\partial\tilde{n}_e} \delta\tilde{n}_e \right)^* \right] \equiv h_r r_{33} + i h_s s_{33}, \quad (18)$$

and separating into real and imaginary parts gives

$$\begin{pmatrix} \delta\psi_{sp} \\ \frac{\delta b}{b} \end{pmatrix} = \begin{pmatrix} \text{Im}(h_r) & \text{Re}(h_s) \\ \text{Re}(h_r) & -\text{Im}(h_s) \end{pmatrix} \begin{pmatrix} r_{33} \\ s_{33} \end{pmatrix}. \quad (19)$$

The functions h_r and h_s are complex quantities given by

$$h_r = iV \left[\left(\frac{k_o \tilde{n}_o^3}{\tilde{n}_e} \sqrt{\tilde{n}_e^2 - N^2} \right)^* \gamma - \frac{k_o \tilde{n}_o^4}{\sqrt{\tilde{n}_o^2 - N^2}} \gamma + \left(\frac{k_o \tilde{n}_o \tilde{n}_e N^2}{\sqrt{\tilde{n}_e^2 - N^2}} \right)^* \right] \quad (20)$$

and

$$h_s = -iV \left[\frac{k_o \tilde{n}_o^4}{\sqrt{\tilde{n}_o^2 - N^2}} \gamma + \left(\frac{k_o \tilde{n}_o^3}{\tilde{n}_e} \sqrt{\tilde{n}_e^2 - N^2} \right)^* \gamma + \left(\frac{k_o \tilde{n}_o \tilde{n}_e N^2}{\sqrt{\tilde{n}_e^2 - N^2}} \right)^* \right], \quad (21)$$

where $N = \sin\theta$ as defined in Eq. (B1) and we have used $r_{13} = \gamma r_{33}$ and $s_{13} = \gamma s_{33}$. The functions h_r and h_s have nonzero real and imaginary parts inside the absorption band. Outside the absorption band, we make the approximations discussed in Appendix A to compare with

formulas reported earlier [12,13,16,20,21]. Then, the 2×2 matrix in Eq. (19) is diagonalized because the real parts of h_r and h_s vanish, and we get

$$\delta\psi_{sp} = -\left(\frac{n_o^4}{\sqrt{n_o^2 - N^2}} - \frac{n_o^3}{n_e} \sqrt{n_e^2 - N^2}\right) k_o \gamma r_{33} V + \frac{n_o n_e N^2}{\sqrt{n_e^2 - N^2}} k_o r_{33} V = \text{Im}(h_r) \cdot r_{33} \quad (22)$$

and

$$\frac{\delta b}{b} = \left(\frac{n_o^4}{\sqrt{n_o^2 - N^2}} + \frac{n_o^3}{n_e} \sqrt{n_e^2 - N^2}\right) k_o \gamma s_{33} V + \frac{n_o n_e N^2}{\sqrt{n_e^2 - N^2}} k_o s_{33} V = -\text{Im}(h_s) \cdot s_{33}, \quad (23)$$

For $n_o \approx n_e \equiv n$, Eqs. (22) and (23) further reduce to

$$\delta\psi_{sp} = \frac{n^2 N^2}{\sqrt{n^2 - N^2}} (1 - \gamma) r_{33} k_o V = \text{Im}(h_r) \cdot r_{33} \quad (24)$$

and

$$\frac{\delta b}{b} = \left(\frac{2n^4 - n^2 N^2}{\sqrt{n^2 - N^2}} \gamma s_{33} + \frac{n^2 N^2}{\sqrt{n^2 - N^2}} s_{33}\right) k_o V = -\text{Im}(h_s) \cdot s_{33}. \quad (25)$$

Equations (22) and (24) are identical with those reported previously [12,21], but our Eqs. (23) and (25) describe the electrochromic effect somewhat differently from that reported in Refs. 13, 16, and 20. In Refs. 13 and 20, the ellipsometric parameter $\tan\Phi$ ($= |r_p/r_s|$) was used to calculate the electrochromic effect, but $\delta|r_s| = 0$ was assumed. In Ref. 16, the variation of complex phase retardation was introduced to estimate the electrochromic effect in the simple model, but their formula for the electrochromic effect is equivalent to that in Refs. 13 and 20 where $\delta|r_s| = 0$ is assumed.

2.3 Rigorous Model

In this section, we use rigorous expressions for the s - and p - reflectance [16, 17, 23]. In the case of a thin film on a TCO-glass substrate, the first reflection off the glass is blocked from reaching the detector [12], as is a second-pass beam resulting from reflection of the first pass on its way out at the glass-air interface back into the polymer and out again. This eliminates reflection fluctuations from the glass layer. Greater care is required to block these beams at high and low angles of incidence, because the transverse separation between reflections becomes narrow at these angles of incidence [24]. If the glass is sufficiently thick, it is possible to block the gross multiple reflections efficiently, i.e., the first reflection off the glass and the second, third, etc passes resulting from back-reflection off the glass-air interface, but it is not generally possible to avoid the multiple reflections inside a thin polymer film. These multiple reflections inside the film are accounted for in the rigorous model but not in the simple model.

Assuming that the incident light is a plane wave, the iteration of the Airy formula [25] gives the reflection coefficient in the whole multilayered sample as shown in Fig. 3(b). As given in Refs. 16 and 17, the resulting expressions for r_s and r_p have the form

$$r = \frac{r_{23} + \hat{r}_{34} e^{2i\beta_3 d_3}}{1 + r_{23} \hat{r}_{34} e^{2i\beta_3 d_3}} \leftarrow \hat{r}_{34} = \frac{r_{34} + \hat{r}_{45} e^{2i\beta_4 d_4}}{1 + r_{34} \hat{r}_{45} e^{2i\beta_4 d_4}} \leftarrow \hat{r}_{45} = \frac{r_{45} + r_{56} e^{2i\beta_5 d_5}}{1 + r_{45} r_{56} e^{2i\beta_5 d_5}}, \quad (26)$$

where we have omitted the s and p subscripts to prevent the notation from becoming unduly cumbersome. In Eq. (26) the s or p propagation constant β_j in each layer j is defined in

Eq. (14) and the corresponding reflection coefficient from layer j to k is given by

$$r_{jk} = \frac{Z_k - Z_j}{Z_k + Z_j} \quad (27)$$

with the s - and p - wave impedances [26] of each layer given by

$$Z^s = \frac{1}{\sqrt{\tilde{n}_o^2 - N^2}}, \quad Z^p = \frac{1}{\tilde{n}_o} \sqrt{1 - \left(\frac{N}{\tilde{n}_e}\right)^2}. \quad (28)$$

In principle, these reflection coefficients should be multiplied by two transmittances, t_{12} and t_{21} , at the air-glass interface [17], but in practice these terms do not contribute to the calculation of $\delta\Psi_{sp}$ and $\delta B/B$ in our analysis. Using Eq. (26), the detailed expressions for the function H that appear in Eq. (11) are given in Appendix C.

2.4 Data Analysis

At a single angle and with knowledge of the linear parameters of the sample structure, the matrix equation shown in Eq. (12) can simply be inverted to solve for r_{33} and s_{33} . Data at multiple angles can be analyzed by solving Eq. (12) for r_{33} and s_{33} at each angle and then calculating mean values for r_{33} and s_{33} . Alternatively, for experimental data at n angles of incidence, we can construct a $2n \times 2$ matrix that is derived by stacking up Eq. (12) to form a large matrix equation

$$\begin{pmatrix} \delta\Psi_{sp}(\theta_1) \\ \vdots \\ \delta\Psi_{sp}(\theta_n) \\ \delta B/B(\theta_1) \\ \vdots \\ \delta B/B(\theta_n) \end{pmatrix} = \begin{pmatrix} \text{Im}[H_r(\theta_1)] & \text{Re}[H_s(\theta_1)] \\ \vdots & \vdots \\ \text{Im}[H_r(\theta_n)] & \text{Re}[H_s(\theta_n)] \\ \text{Re}[H_r(\theta_1)] & -\text{Im}[H_s(\theta_1)] \\ \vdots & \vdots \\ \text{Re}[H_r(\theta_n)] & -\text{Im}[H_s(\theta_n)] \end{pmatrix} \begin{pmatrix} r_{33} \\ s_{33} \end{pmatrix} \Leftrightarrow P = M \cdot x. \quad (29)$$

It is easy to calculate r_{33} and s_{33} simultaneously using several matrix decomposition methods such as QR and singular value decomposition to implement least squares fitting [27]. Using QR decomposition, the matrix M can be decomposed into Q and R which are $2n \times 2n$ orthogonal and $2n \times 2$ upper triangular matrices, respectively and we define \hat{P} as

$$M \cdot x = P \Rightarrow QR \cdot x = P \Rightarrow R \cdot x = Q^T P \equiv \hat{P}. \quad (30)$$

Taking the 2×2 upper triangular matrix from R and the 2×1 upper matrix from \hat{P} allows one to obtain x ,

$$R \cdot x = \hat{P} \Rightarrow \begin{pmatrix} R_{2 \times 2} \\ R_{lower} \end{pmatrix} \cdot x = \begin{pmatrix} P_{2 \times 1} \\ P_{lower} \end{pmatrix} \Rightarrow x = R_{2 \times 2}^{-1} \cdot P_{2 \times 1}, \quad (31)$$

where R_{lower} is the $(2n-2) \times 2$ null matrix and the magnitude of P_{lower} represents the goodness of least squares fitting. Because the linear parameters (including the refractive index and thickness of the film) that determine the H functions have experimental errors associated with

their measurement, it is possible to tweak their values within their experimental uncertainty range and recalculate Eqs. (29)-(31) to attempt to improve the goodness of fit of r_{33} and s_{33} . Ref. 17 followed a more complicated approach by finding numerical fits to the rigorous expressions using the simplex method to fit the modulated intensities at three bias points as a function of angle. The complex variations of refractive indices as shown in Eq. (1) were not taken into account although it should be included for a highly absorptive medium.

3. Results

In this section, we estimate the relative error that results from using the simple model for a number of different cases. Assuming the rigorous model gives the correct value, the relative error is defined as

$$Error = \frac{r_{33}^{SM} - r_{33}}{r_{33}}. \quad (32)$$

For a given modulated phase and reflectivity, r_{33} and s_{33} from the rigorous model are calculated from Eq. (12) together with Eqs. (C1) and (C2), while the simple model values r_{33}^{SM} and s_{33}^{SM} are calculated from Eqs. (19)-(21). To evaluate the error we equate the right hand sides of Eqs. (12) and (19) and rearrange to obtain

$$Error = \frac{\text{Im}(h_s)[\text{Im}(H_r) - \text{Im}(h_r)] + \text{Re}(h_s)[\text{Re}(H_r) - \text{Re}(h_r)]}{\text{Im}(h_r)\text{Im}(h_s) + \text{Re}(h_r)\text{Re}(h_s)} + \frac{\text{Im}(h_s)\text{Re}(H_s) - \text{Re}(h_s)\text{Im}(H_s)}{\text{Im}(h_r)\text{Im}(h_s) + \text{Re}(h_r)\text{Re}(h_s)} \frac{s_{33}}{r_{33}}. \quad (33)$$

The result depends on the ratio s_{33}/r_{33} , but not on the absolute magnitude of either coefficient. Outside the absorption band of the polymer, $\text{Re}(h_r) = \text{Re}(h_s) = 0$ for the simple model as discussed in Sec. 2.2.

For the first case, we consider the example of a sample structure with a thick gold electrode where the index of the nonlinear film and the TCO are matched with the glass substrate under the assumption of no electrochromic effect and no optical loss in the polymer or TCO layer. That is, $n_2 = n_3 = n_4 = 1.5$ in the absence of an applied voltage. One might think that the simple model should apply exactly in this case, but the index matching condition is broken upon application of a voltage leading to some reflectivity modulation, which is ignored in the simple model. Using $r_{23} = r_{34} = 0$ and $\hat{r}_{45} = r_{45}$ (valid for gold thicker than ~ 75 nm), the reflection coefficient in Eq. (26) simplifies to

$$r = r_{45} e^{2i\beta_3 d_3} e^{2i\beta_4 d_4}, \quad (34)$$

and the f 's and g 's in Eq. (C7) are

$$f_{234}^q = e^{2i\beta_3 d_3}, f_{345}^q = e^{2i\beta_4 d_4}, g_{345}^q = 1 - (r_{45}^q)^2 e^{2i\beta_4 d_4}, g_{456}^q = 1. \quad (35)$$

Then, H_r in Eq. (C1) can be expressed as

$$H_r \equiv -\frac{V(n_4)^3}{2d_4} [K_1 \cos(2\beta_4 d_4) - iK_2 \sin(2\beta_4 d_4) + K_3] - iV(n_4)^3 K_4, \quad (36)$$

where

$$\begin{aligned}
K_1 &= \left[1 - (r_{45}^s)^2 \right] \frac{\gamma}{r_{45}^s} \frac{\partial r_{34}^s}{\partial \tilde{n}_o} + \left[1 - (r_{45}^{p*})^2 \right] \left(\frac{\gamma}{r_{45}^{p*}} \frac{\partial r_{34}^p}{\partial n_o} + \frac{1}{r_{45}^{p*}} \frac{\partial r_{34}^p}{\partial \tilde{n}_e} \right) \\
K_2 &= \left[1 + (r_{45}^s)^2 \right] \frac{\gamma}{r_{45}^s} \frac{\partial r_{34}^s}{\partial \tilde{n}_o} - \left[1 + (r_{45}^{p*})^2 \right] \left(\frac{\gamma}{r_{45}^{p*}} \frac{\partial r_{34}^p}{\partial n_o} + \frac{1}{r_{45}^{p*}} \frac{\partial r_{34}^p}{\partial \tilde{n}_e} \right) \\
K_3 &= \frac{\gamma}{r_{45}^s} \frac{\partial r_{45}^s}{\partial \tilde{n}_o} + \frac{\gamma}{r_{45}^{p*}} \frac{\partial r_{45}^{p*}}{\partial n_o} + \frac{1}{r_{45}^{p*}} \frac{\partial r_{45}^{p*}}{\partial \tilde{n}_e} \\
K_4 &= \gamma \frac{\partial \beta_{4s}}{\partial \tilde{n}_o} - \gamma \frac{\partial \beta_{4p}}{\partial n_o} - \frac{\partial \beta_{4p}}{\partial \tilde{n}_e},
\end{aligned} \tag{37}$$

and the derivatives in these expressions are given in Eqs. (C8)-(C10). The first two terms in Eq. (36) are due to modulation of the reflectivity at the TCO-polymer interface and contribute oscillation as the thickness d_4 of the polymer film changes, while the third term is due to modulation of the reflectivity of the polymer-gold interface and contributes an offset. The terms involving the complex quantities K_1 , K_2 , and K_3 are inversely proportional to the film thickness, but the last term involving the real quantity K_4 is independent of film thickness and equal to h_r in the simple model shown in Eq. (24). With $s_{33} = 0$, the error expression Eq. (33) takes the form

$$Error = \frac{1}{2d_4 K_4} \left[\text{Im}(K_1) \cos(2\beta_4 d_4) - \text{Re}(K_2) \sin(2\beta_4 d_4) + \text{Im}(K_3) \right]. \tag{38}$$

The error percentage is plotted as a function of film thickness in Fig. 4. Notable is that the error oscillates from overestimation to underestimation and the envelope decreases with increasing thickness.

As other cases, we consider the relative error for different refractive index and thickness combinations of the polymer film for selected values of complex index and thickness of ITO at four wavelengths, 0.8, 1, 1.3, and 1.55 μm and the ratio s_{33}/r_{33} is assumed to be 1 and 2 at 0.8 μm , and to be 0.1 at wavelengths 1, 1.3, and 1.55 μm for the simulation. The complex index of refraction of ITO measured by ellipsometry and the complex index of refraction of a representative doped NLO polymer film are shown in Fig. 5. The optical properties of ITO are strongly dependent on the manufacturing process so there are wide variations in commercial ITO properties. Free carrier absorption is usually noticeable in the near infrared range, whereas interband transitions dominate in the visible range [28]. The gold metal layer is

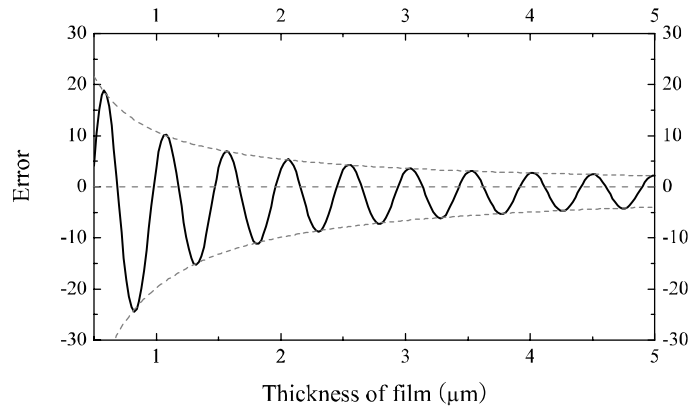


Fig 4. Error percentage plot for varying film thickness when the refractive indices of film and TCO are matched with glass ($n = 1.5$) at 1.3 μm wavelength. The positive and negative envelopes are proportional to $\pm 1/d_4$ with a negative offset.

assumed to be thicker than $\sim 75\text{nm}$ because we have found that for thicknesses greater than this the thickness of the gold layer can be ignored because no light is reflected back from the gold/air interface.

Figure 6 shows the error plots as a function of thickness of the polymer for polymer indices of refraction shown in Fig. 5 (ignoring birefringence). Noteworthy is that for a given refractive index, the error cycles from positive to negative (overestimation to underestimation) as a function of film thickness when the loss of the film is negligible as shown in Figs. 6(b)-6(d) and 6(f)-6(h). This is because increasing the thickness causes a periodic phase retardation. The error extremes also tend to increase as the wavelength increases because the ITO becomes more

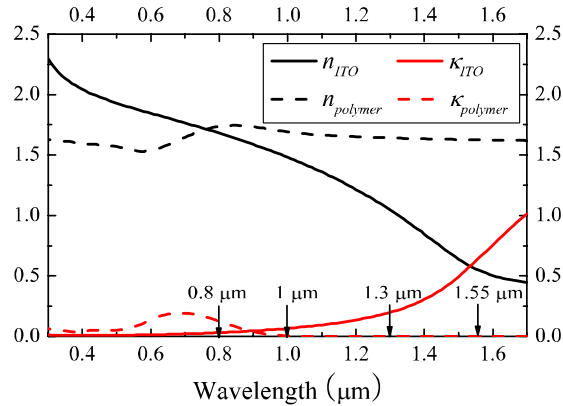


Fig. 5. Optical properties ($n+i\kappa$) of (solid) a representative ITO (Abrisa Corporation) measured by ellipsometry and (dashed) a representative polymer film selected for the simulation. (real part : black, imaginary part : red).

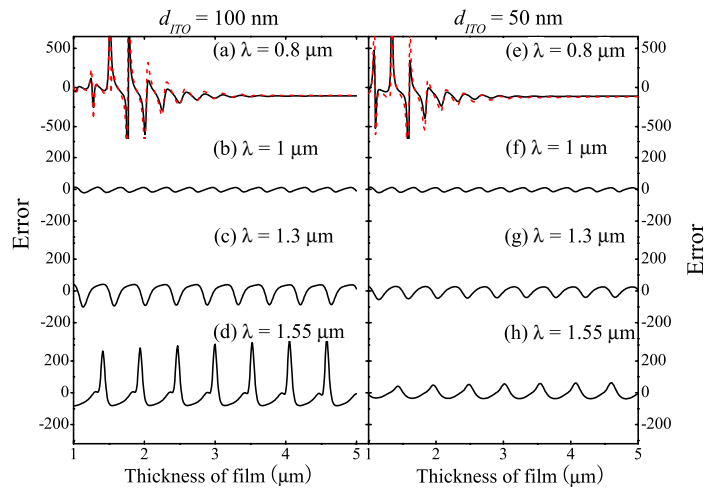


Fig. 6. Error plots by varying the thickness of the film for fixed indices of refraction of ITO and the film and two thicknesses of ITO, 100 nm (a-d) and 50 nm (e-h) at various wavelengths and 45° angle of incidence under assumption of $\gamma = 1/3$. For plots (a) and (e), $s_{33}/r_{33} = 1$ (black solid), and $s_{33}/r_{33} = 2$ (red dashed). For the wavelengths other than $0.8 \mu\text{m}$, values of s_{33}/r_{33} between 0 and 0.1 produce curves that are indistinguishable on this scale. For (a) and (e), the errors approach -107% and -110% , respectively. For (b), (f), (c), (g), (d), and (h), the error extremes are -18% to 12% , -15% to 10% , -86% to 38% , -40% to 25% , -80% to 350% , and 37% to 63% , respectively.

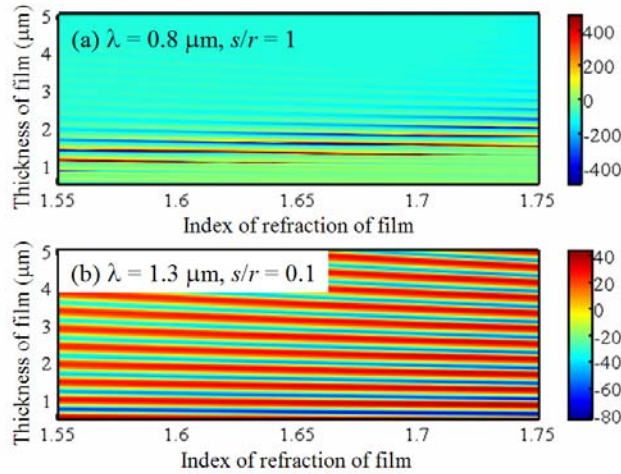


Fig. 7. Error contour plots at (a) $\lambda = 0.8 \mu\text{m}$ and $s_{33}/r_{33} = 1$ (b) $\lambda = 1.3 \mu\text{m}$ and $s_{33}/r_{33} = 0.1$ with thickness of ITO = 100 nm, 45° angle of incidence, and $\gamma = 1/3$. Each contour plot (a) and (b) shows asymptotic and cyclic behaviors with thickness of film irrespective of index of refraction of film, respectively.

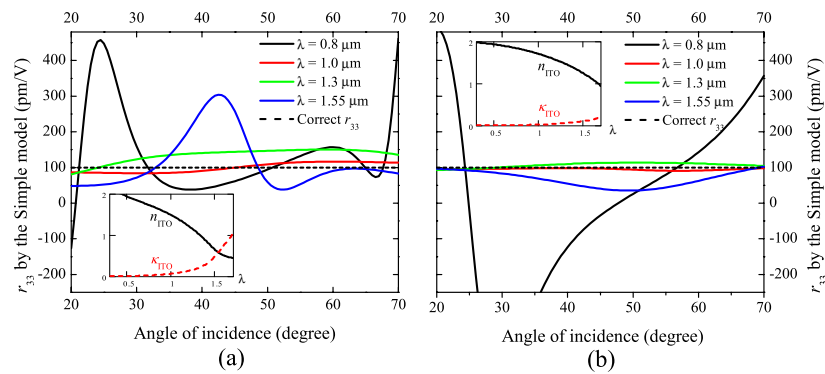


Fig. 8. EO coefficients r_{33} calculated by the simple model at various wavelengths and angles of incidence using thickness of film and ITO, 1.4 μm and 100 nm, respectively. EO coefficient $r_{33} = 100 \text{ pm/V}$ was used for the simulation. The ratios s_{33}/r_{33} are 2 at 0.8 μm and 0.1 at the other wavelength. Insets in (a) and (b) show the optical properties of ITO selected for the simulation. The crossover points of n and κ of ITO are around 1.54 and 1.92 μm in (a) and (b), respectively.

reflective, which enhances FP effects inside the polymer layer. Thicker ITO also tends to increase the reflectivity. When the operating wavelength is in the absorption band of the polymer film as shown in Figs. 6(a) and 6(e), the error initially fluctuates irregularly when the film is thin and finally converges to a constant negative value as the film thickness increases. This is because propagation loss in the film has a dual effect of reducing multiple reflections as well as reducing the relative amount of phase modulation from the polymer bulk compared to the phase modulation of the light reflected from ITO/polymer interface, which is not accounted for in the simple model. Within the absorption band, a thick film results in a constant error, but the correct value is not predictable without the rigorous analysis.

The error in using the simple model versus the film thickness shows qualitatively similar behavior irrespective of the index of refraction of the film as shown in Figs. 7(a) and 7(b). We also note, contrary to earlier suggestions [16,18], that the error from using the simple model is not in general reduced by using film thicknesses on the order of a wavelength or less.

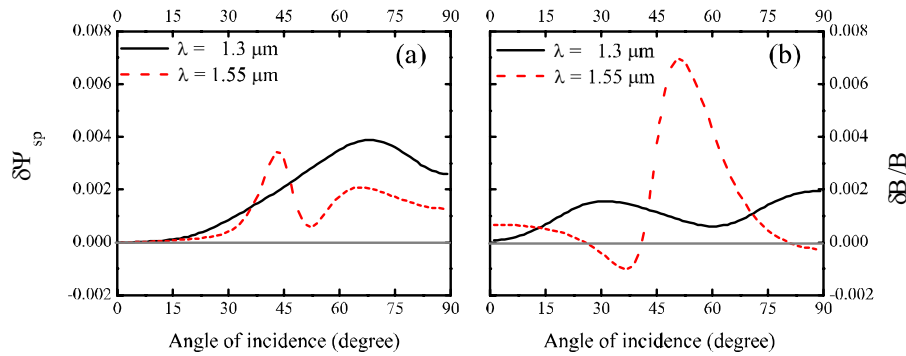


Fig. 9. (a) $\delta\Psi_{sp}$ and (b) $\delta B/B$ versus angle of incidence at wavelengths 1.3 and 1.55 μm . The ratio $s_{33}/r_{33} = 0.1$ and film thickness = 1.4 μm were used at both wavelengths for the ITO properties shown in Fig. 5.

Figure 8 shows simple model r_{33} values as a function of angle of incidence for two different ITO samples where the ITO for Fig. 8(b) is less reflective than for Fig. 8(a). In Fig. 8(a), most EO coefficients calculated by the simple model with varying angle of incidence are far away from the correct r_{33} . Note that although the simple model EO coefficient values seem to be flat at 1.3 μm for angles of incidence between 30° and 60°, they are nevertheless overestimated by about 50%. Thus, obtaining nearly constant simple model r_{33} values as a function of angle of incidence does not guarantee the value is correct. When the ITO is less absorptive as shown in the inset of Fig. 8(b), the correct r_{33} is approached for wavelengths of 1 and 1.3 μm because these wavelengths are in a spectral region where both polymer and ITO are more transparent.

In Fig. 9(a) and 9(b), the simulated $\delta\Psi_{sp}$ and $\delta B/B$ are plotted at wavelengths 1.3 and 1.55 μm using the rigorous model. We notice that the $\delta\Psi_{sp}$'s are quite different from those of the simple Teng-Man method [13, 20]. Also, $\delta B/B$ at a wavelength of 1.55 μm passes through 0 at several angles of incidence. Thus, measuring $\delta B/B = 0$ at a fixed angle of incidence does not mean that there is no electrochromic effect, contrary to the suggestion in Ref. 16. We observe that $\delta\Psi_{sp}$ and $\delta B/B$ fluctuate more at 1.55 μm than at 1.3 μm because of the more reflective ITO.

For those making Teng-Man measurements and desiring accuracies of only $\pm 20\%$, we identify in Table 1 sets of ranges of the refractive indices and thicknesses of the layers that have been found to allow at least this accuracy using just the simple model and measurements at a 45° angle of incidence under assumption of no loss and no electrochromic effect in the film. As can be seen from Fig. 6, the error in using the simple model oscillates from positive to negative going through zero at isolated points. Thus, there can be particular combinations of parameters outside the table ranges that give an error better than $\pm 20\%$, but the table has been constructed to keep the envelope of the error oscillation within $\pm 20\%$. The rigorous model should be used when the parameters are outside these ranges, or when accuracy better than $\pm 20\%$ is desired.

4. Conclusions

In this paper, we have presented new mathematical expressions for analyzing Teng-Man data in both transparent and absorptive films that take into account the optical properties of the TCO layer. The formulas presented were derived using a rigorous model that includes the effect of multiple reflections inside the multilayered structure at any angle of incidence. In addition, a new expression has been derived for the electrochromic effect in a simple model. A curve fitting procedure has been described for the full profiles of angle dependent I_{dc} and I_m to extract more accurate complex EO coefficient values from the experimental data. Based on linear least squares fitting, this method is expected to facilitate the use of a rigorous model to

Table 1. Parameter ranges to use the simple model with error less than $\pm 20\%$ at 45° angle of incidence.

n_{film}	λ (μm)	n_{TCO}	κ_{TCO}	d_{TCO} (nm)	d_{film} (μm) ^a
1.5-1.6	1.0	1.4 - 2.0	< 0.1	< 60	> 2.0
	1.3	1.3 - 2.0	< 0.6	< 40	> 1.8
	1.55	1.3 - 2.0	< 0.5	< 40	> 2.0
1.6-1.7	1.0	1.5 - 1.9	< 0.1	< 60	> 2.0
	1.3	1.4 - 2.0	< 0.4	< 40	> 2.0
	1.55	1.4 - 2.0	< 0.6	< 40	> 1.9
1.7-1.8	1.0	1.6 - 1.9	< 0.1	< 40	> 3.2
	1.3	1.6 - 2.0	< 0.28	< 30	> 2.6
	1.55	1.5 - 2.0	< 0.36	< 30	> 2.6

^aSimulated up to 1 μm larger than the given minimum thickness.

obtain reliable EO coefficients for poled Teng-Man samples. In order to use the rigorous model, however, it is necessary to know detailed information about the sample because simultaneously fitting multiple parameters does not give a unique fit. We have shown that the relative error from using the simple model can experience cyclic, asymptotic, and irregular behaviors depending on the operating wavelength as the thickness of the polymer film increases. The error extremes can be reduced by choosing an operating wavelength where the absorption of the polymer and TCO are small simultaneously, not by decreasing the thickness of the polymer film on the order of a wavelength or less. We also note that the complex quadratic EO coefficient can be measured by detecting the signal at twice the fundamental frequency or by applying a DC offset to the polymer film with a sinusoidal bias as discussed in Ref. 20. Our formulas can easily be modified to include these effects. We also expect that our analysis can be applied to the interferometric types of measurement to estimate the relative error introduced by the TCO layer.

Acknowledgments

The authors gratefully acknowledge the support of the DARPA MORPH program and the Laboratory for Physical Sciences. We thank Alex K.-Y. Jen and Larry Dalton for providing some of the ITO and polymer samples, Bob Norwood for discussions on ITO properties, Mike Hayden for initial discussions on Teng-Man measurements, Younggu Kim for assistance with ellipsometry and UV-VIS-NIR, and Victor Yun for assistance in construction of Teng-Man setup.

Appendix A: Variation of index of refraction

In this appendix, we discuss the dependence of the variation of the real and imaginary parts of the complex refractive index on the $r_{\mu 3}$ and $s_{\mu 3}$ coefficients. Separation of Eq. (1) into real and imaginary parts gives

$$\delta n_{\mu} = -\frac{n_{\mu}^3}{2} \left[\left(1 - 3 \frac{\kappa_{\mu}^2}{n_{\mu}^2} \right) r_{\mu 3} + \left(\frac{\kappa_{\mu}^2}{n_{\mu}^2} - 3 \right) \frac{\kappa_{\mu}}{n_{\mu}} s_{\mu 3} \right] E_3 \quad (\text{A1})$$

and

$$\delta \kappa_{\mu} = -\frac{n_{\mu}^3}{2} \left[\left(1 - 3 \frac{\kappa_{\mu}^2}{n_{\mu}^2} \right) s_{\mu 3} + \left(\frac{\kappa_{\mu}^2}{n_{\mu}^2} - 3 \right) \frac{\kappa_{\mu}}{n_{\mu}} r_{\mu 3} \right] E_3. \quad (\text{A2})$$

It can be seen that the change in both the real and imaginary parts of the refractive index depends in general on both the real and imaginary parts of the electro-optic coefficients.

Even for a highly absorptive medium, at communication wavelengths the extinction coefficient is small (10 dB/cm loss corresponds to an extinction coefficient $\kappa = 0.000024$) so $\kappa/n \ll 1$ is a reasonable approximation. With these considerations in mind, for communication wavelengths in the 1300-1600 nm range, Eqs. (A1) and (A2) can be simplified to

$$\delta n_\mu \approx -\frac{1}{2} n_\mu^3 \left(r_{\mu 3} - 3 \frac{\kappa_\mu}{n_\mu} s_{\mu 3} \right) E_3 \quad (\text{A3})$$

and

$$\delta \kappa_\mu \approx -\frac{1}{2} n_\mu^3 \left(s_{\mu 3} + 3 \frac{\kappa_\mu}{n_\mu} r_{\mu 3} \right) E_3. \quad (\text{A4})$$

Outside the absorption band, we expect $r_\mu \gg 3(\kappa_\mu / n_\mu) s_\mu$, which simplifies Eq. (A3) to

$$\delta n_\mu \approx -\frac{1}{2} n_\mu^3 r_{\mu 3} E_3. \quad (\text{A5})$$

Furthermore, still outside the absorption band, the assumption $s_\mu \gg 3(\kappa_\mu / n_\mu) r_\mu$ reduces Eq. (A4) to

$$\delta \kappa_\mu \approx -\frac{1}{2} n_\mu^3 s_{\mu 3} E_3. \quad (\text{A6})$$

We note that the conditions $r_\mu \gg 3(\kappa_\mu / n_\mu) s_\mu$ and $s_\mu \gg 3(\kappa_\mu / n_\mu) r_\mu$ are equivalent to those in Ref. [13] and Eqs. (A5) and (A6) are valid outside the polymer absorption band. Consequently, δn and $\delta \kappa$ depend only on r_{33} and s_{33} , respectively. Within the absorption band of the polymer, however, this is not true and Eq. (1) or, equivalently, Eqs. (A1) and (A2) should be used.

Appendix B: Variation of the propagation constants inside the nonlinear film

Here, we give the detailed expressions for the variation of the s - and p -wave propagation constants. From Snell's law we have

$$\tilde{n}_s \sin \tilde{\theta}_s = \tilde{n}_p \sin \tilde{\theta}_p = \sin \theta \equiv N, \quad (\text{B1})$$

where $\tilde{n}_s = \tilde{n}_o$ and

$$\frac{1}{\tilde{n}_p^2} = \frac{\cos^2 \tilde{\theta}_p}{\tilde{n}_o^2} + \frac{\sin^2 \tilde{\theta}_p}{\tilde{n}_e^2}. \quad (\text{B2})$$

Using N , which is of course constant at a given angle of incidence, we can write the propagation constants in the forms

$$\beta_s = k_o \sqrt{\tilde{n}_o^2 - N^2} \quad (\text{B3})$$

and

$$\beta_p = k_o \frac{\tilde{n}_o}{\tilde{n}_e} \sqrt{\tilde{n}_e^2 - N^2}. \quad (\text{B4})$$

An advantage of expressing the β 's in terms of N is that we do not have to explicitly deal with changes in the internal angles θ_s and θ_p as the refractive index changes, they are automatically accounted for in this representation.

The variations of $\beta_{s,p}$ induced by the applied voltage are given by

$$\delta\beta_s = \frac{k_o \tilde{n}_o}{\sqrt{\tilde{n}_o^2 - N^2}} \delta\tilde{n}_o \quad (\text{B5})$$

and

$$\delta\beta_p = \frac{k_o}{\tilde{n}_e} \sqrt{\tilde{n}_e^2 - N^2} \delta\tilde{n}_o + \frac{k_o \tilde{n}_o N^2}{\tilde{n}_e^2 \sqrt{\tilde{n}_e^2 - N^2}} \delta\tilde{n}_e. \quad (\text{B6})$$

Outside the absorption band, we can make the approximations discussed in Appendix A to obtain

$$\delta\beta_s \approx \frac{k_o n_o}{\sqrt{n_o^2 - N^2}} (\delta n_o + i\delta\kappa_o) \quad (\text{B7})$$

and

$$\delta\beta_p \approx \frac{k_o}{n_e} \sqrt{n_o^2 - N^2} (\delta n_o + i\delta\kappa_o) + \frac{k_o N^2 n_o}{n_e^2 \sqrt{n_e^2 - N^2}} (\delta n_e + i\delta\kappa_e). \quad (\text{B8})$$

Appendix C: H functions in the rigorous model

In this appendix, we derive detailed expressions for the functions H_r and H_s that appear in Eq. (11) and describe the linear dependence of $\delta\tilde{B}/\tilde{B}$ on r_{33} and s_{33} for the rigorous expression of reflectance. Also, because many software analysis packages can handle complex numbers efficiently, we retain the complex expressions for $\delta\tilde{n}_o$ and $\delta\tilde{n}_e$ as described in Eq. (1).

Performing the operations described in Eq. (11), we have

$$H_r = -\frac{V}{2d_4} \left[\frac{\gamma}{r_s} \frac{\partial r_s}{\partial \tilde{n}_o} \tilde{n}_o^3 + \gamma \left(\frac{1}{r_p} \frac{\partial r_p}{\partial \tilde{n}_o} \tilde{n}_o^3 \right)^* + \left(\frac{1}{r_p} \frac{\partial r_p}{\partial \tilde{n}_e} \tilde{n}_e^3 \right)^* \right] \quad (\text{C1})$$

and

$$H_s = -\frac{V}{2d_4} \left[\frac{\gamma}{r_s} \frac{\partial r_s}{\partial \tilde{n}_o} \tilde{n}_o^3 - \gamma \left(\frac{1}{r_p} \frac{\partial r_p}{\partial \tilde{n}_o} \tilde{n}_o^3 \right)^* - \left(\frac{1}{r_p} \frac{\partial r_p}{\partial \tilde{n}_e} \tilde{n}_e^3 \right)^* \right]. \quad (\text{C2})$$

Next, we derive detailed expressions for the derivatives in Eqs. (C1) and (C2) using the rigorous reflection coefficients r_s and r_p . Expanding Eq. (26), we see that the required derivatives in Eqs. (C1) and (C2) are off the form

$$\frac{1}{r} \frac{\partial r}{\partial \tilde{n}_{o,e}} = \frac{1}{r} \frac{\partial r}{\partial \hat{r}_{34}} \left(\frac{\partial \hat{r}_{34}}{\partial r_{34}} \frac{\partial r_{34}}{\partial \tilde{n}_{o,e}} + \frac{\partial \hat{r}_{34}}{\partial \hat{r}_{45}} \frac{\partial \hat{r}_{45}}{\partial r_{45}} \frac{\partial r_{45}}{\partial \tilde{n}_{o,e}} + \frac{\partial \hat{r}_{34}}{\partial \beta_4} \frac{\partial \beta_4}{\partial \tilde{n}_{o,e}} \right), \quad (\text{C3})$$

where we have omitted the s, p designations to prevent the notation from becoming unduly cumbersome. The three derivatives with respect to \tilde{n}_o and \tilde{n}_e are given by

$$\frac{1}{r_s} \frac{\partial r_s}{\partial \tilde{n}_o} = \frac{f_{234}^s}{r_s} \left(g_{345}^s \frac{\partial r_{34}^s}{\partial \tilde{n}_o} + f_{345}^s g_{456}^s \frac{\partial r_{45}^s}{\partial \tilde{n}_o} + 2id_4 \hat{r}_{45}^s f_{345}^s \frac{\partial \beta_{s4}}{\partial \tilde{n}_o} \right), \quad (\text{C4})$$

$$\frac{1}{r_p} \frac{\partial r_p}{\partial \tilde{n}_o} = \frac{f_{234}^p}{r_p} \left(g_{345}^p \frac{\partial r_{34}^p}{\partial \tilde{n}_o} + f_{345}^p g_{456}^p \frac{\partial r_{45}^p}{\partial \tilde{n}_o} + 2id_4 \hat{r}_{45}^p f_{345}^p \frac{\partial \beta_{p4}}{\partial \tilde{n}_o} \right), \quad (\text{C5})$$

and

$$\frac{1}{r_p} \frac{\partial r_p}{\partial \tilde{n}_e} = \frac{f_{234}^p}{r_p} \left(g_{345}^p \frac{\partial r_{34}^p}{\partial \tilde{n}_e} + f_{345}^p g_{456}^p \frac{\partial r_{45}^p}{\partial \tilde{n}_e} + 2i d_4 \hat{r}_{45}^p f_{345}^p \frac{\partial \beta_{p4}}{\partial \tilde{n}_e} \right), \quad (C6)$$

where the f 's and g 's are defined by

$$f_{ijk}^q = \frac{\left[1 - (r_{ij}^q)^2 \right] \exp(2i\beta_{qj} d_j)}{\left[1 + r_{ij}^q \hat{r}_{jk}^q \exp(2i\beta_{qj} d_j) \right]^2}, \quad g_{ijk}^q = \frac{1 - (\hat{r}_{jk}^q)^2 \exp(4i\beta_{qj} d_j)}{\left[1 + r_{ij}^q \hat{r}_{jk}^q \exp(2i\beta_{qj} d_j) \right]^2} \quad (C7)$$

with $q = s, p$. The remaining derivatives in Eqs. (C4)-(C6) are given by

$$\frac{\partial r_{34}^s}{\partial \tilde{n}_o} = \frac{-2\tilde{n}_o Z_3^s (Z_4^s)^3}{(Z_3^s + Z_4^s)^2}, \quad \frac{\partial r_{34}^p}{\partial \tilde{n}_o} = \frac{-2Z_3^p Z_4^p}{\tilde{n}_o (Z_3^p + Z_4^p)^2}, \quad \frac{\partial r_{34}^p}{\partial \tilde{n}_e} = \frac{2Z_3^p N^2}{\tilde{n}_o^2 \tilde{n}_e^3 Z_4^p (Z_3^p + Z_4^p)^2}, \quad (C8)$$

$$\frac{\partial r_{45}^s}{\partial \tilde{n}_o} = \frac{2\tilde{n}_o (Z_4^s)^3 Z_5^s}{(Z_4^s + Z_5^s)^2}, \quad \frac{\partial r_{45}^p}{\partial \tilde{n}_o} = \frac{2Z_4^p Z_5^p}{\tilde{n}_o (Z_4^p + Z_5^p)^2}, \quad \frac{\partial r_{45}^p}{\partial \tilde{n}_e} = \frac{-2Z_5^p N^2}{\tilde{n}_o^2 \tilde{n}_e^3 Z_4^p (Z_4^p + Z_5^p)^2}, \quad (C9)$$

and

$$\frac{\partial \beta_{s4}}{\partial \tilde{n}_o} = k_o Z_4^s \tilde{n}_o, \quad \frac{\partial \beta_{p4}}{\partial \tilde{n}_o} = k_o Z_4^p \tilde{n}_o, \quad \frac{\partial \beta_{p4}}{\partial \tilde{n}_e} = k_o \frac{1}{Z_4^p} \left(\frac{N^2}{\tilde{n}_e^3} \right). \quad (C10)$$

Here, the wave impedance Z 's are defined in Eq. (28).

For writing a computer program, it is straightforward to start with the definition of the wave impedance Z 's in Eq. (28) and substitute from Eq. (C10) sequentially back to Eqs. (C1) and (C2) using also the definition of the total reflection coefficients r_s and r_p from Eq. (26). However, it is in general unduly cumbersome to express the functions H_r and H_s in Eqs. (C1) and (C2) as explicit functions of the linear parameters (complex refractive index and thickness) of the multilayer sample structure.